

INTERACTION OF LASER RADIATION WITH MATTER

PACS numbers: 81.05.ue; 79.20.Ds; 79.20.Eb
DOI: 10.1070/QE2015v045n12ABEH015919

Water at the graphene–substrate interface: interaction with short laser pulses

V.D. Frolov, E.V. Zavedeev, P.A. Pivovarov, A.A. Khomich, A.N. Grigorenko, V.I. Konov

Abstract. **We have investigated the role of adsorption water in the local transformation of multilayer graphene deposited on an oxidised silicon substrate, which was exposed to nanosecond low-intensity focused laser radiation with a wavelength of 532 nm in the air. Experimental data obtained for a laser energy density $E = 0.04$ J cm^{-2} suggest that the formation of micropits (craters) is a consequence of the multipulse removal of the layer of a water adsorbate, which is intercalated between graphene and the substrate, from the zone of laser irradiation of the graphene sheet. The energy threshold of graphene damage in the regions devoid of water was found to be higher in comparison with the initial one (0.058 against 0.048 J cm^{-2}). According to computer simulations of the heating dynamics of the sample and the heat distribution in the substrate–adsorbate–graphene multilayer system, at energy densities corresponding to the experimental ones the water adsorbate layer heats to a temperature sufficiently high to form an increased-pressure vapour cavity under the graphene film.**

Keywords: *graphene, water adsorbate, laser radiation, profiling.*

1. Introduction

Graphene, a two-dimensional layer of carbon atoms, belongs to the class of nanostructures whose physical properties depend heavily on the properties of the ambient medium. Of special interest is the interaction of graphene with water. Quite common is the situation whereby water is adsorbed and retained in micropores. The use of this low-dimensional water underlies the processes that will make possible promising technologies in materials sciences and biology, tribology and nanotechnology [1–4]. The presence of a water adsorbate on the graphene surface is capable of 'opening' its forbidden band and markedly changing the conductivity, in particular by way of efficient doping. Specifically, by adsorbing water from the atmosphere it has been possible to broaden the graphene band gap to about 0.2 eV [5]; spontaneous doping was repeatedly observed with graphene samples deposited on Si/SiO_x substrates with the use of Raman scattering (RS) spectroscopy techniques [6, 7].

Our previous experiments [8] were indicative of another interesting effect, which may be caused by the influence of the water adsorbate. We found that micropits and microholes may be formed in a multilayer graphene sheet under multiple pulsed laser irradiation with intensities much lower than the threshold of the graphene (graphite) damage by single laser pulses. The depth of such micropits did not exceed the graphene sheet thickness and their diameter was slightly larger than the irradiation spot size. To explain this effect, we hypothesised that the microstructuring of graphene was caused by the heating, boiling and forcing out (along the temperature and pressure gradient) of the adsorbed water layer residing between the graphene sheet and the substrate.

The objective of the present work was to verify the assumption of the decisive role of the water adsorbate in microprofiling the multilayer graphene sheet on the substrate by conducting dedicated experiments and numerical estimates of pulsed laser heating of the adsorbate in the layered system graphene–adsorbate–silicon oxide–silicon substrate. Discovered and investigated in this case was an attendant effect: an improvement in damage resistance of the graphene area which had been earlier exposed to a series of low-intensity laser pulses.

2. Experiment

For an object of pulsed laser irradiation we selected multilayer graphene obtained by defoliation and transferred onto an oxidised silicon plate in the air (the thickness of the SiO_2 oxide film was equal to about 300 nm). The resultant film consisted of graphene flakes 3–7 μm in size. The number of layers in each flake was monitored by the RS technique.

Typical RS spectra are depicted in Fig. 1. In the 2D peak of RS by the graphene flake under investigation, one can see two humps of about equal height [curve (*1*)], which are shifted to the long-wavelength side in comparison with the peak for graphite [curve (*3*)]. This RS spectrum is characteristic for 3–6-layer graphene [9]. Also shown for comparison in Fig. 1 is the RS spectrum for single-layer graphene [curve (*2*)]. It is noteworthy that the presence of the water adsorbate on the graphene surface has no influence of any significance on the RS spectrum of graphene [10].

The samples were irradiated by the second harmonic of Nd:YAG laser radiation with the same parameters as in Ref. [8]: wavelength, $\lambda = 532$ nm; pulse duration, $\tau = 10$ ns; repetition rate, 1000 Hz. The laser beam was incident along the normal to the graphene surface and focused to a spot of

V.D. Frolov, E.V. Zavedeev, P.A. Pivovarov, V.I. Konov
A.M. Prokhorov General Physics Institute, Russian Academy of Sciences, ul. Vavilova 38, 119991 Moscow, Russia; National Research Nuclear University 'MEPhI', Kashirskoe sh. 31, 115409 Moscow, Russia; e-mail: p_pivovarov@hotmail.com;
A.A. Khomich A.M. Prokhorov General Physics Institute, Russian Academy of Sciences, ul. Vavilova 38, 119991 Moscow, Russia;
A.N. Grigorenko Manchester Centre for Mesoscience and Nanotechnology, University of Manchester, Oxford Road, Manchester M13 9PL, UK

Received 12 August 2015
Kvantovaya Elektronika **45** (12) 1166–1170 (2015)
Translated by E.N. Ragozin

diameter $d_0 \approx 0.5\ \mu$m. The irradiation pulse energy (E) density was varied in the range 0.04–0.06 J cm^{-2}. The samples were placed in a NTEGRA Spectra M scanning probe microscope. Prior to and after irradiation, the relief of the graphene sheet was monitored in a tapping mode with a lateral resolution of about 10 nm and a resolution of about 0.1 nm along the optical axis. In the majority of experiments, the laser irradiation and the measurements were carried out at room temperature and a relative air humidity RH ≈ 25%. In test experiments, prior to irradiation the samples were aged in a chamber for RH ≈ 90% for seven days.

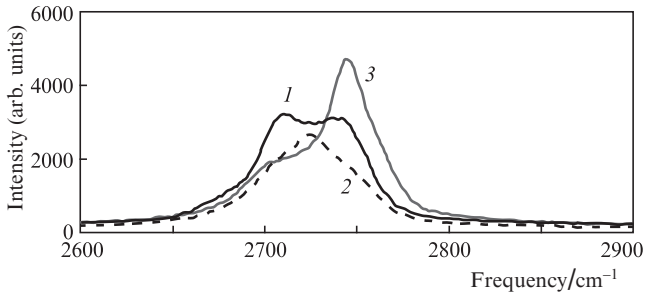

Figure 1. RS spectra for the experimental sample in the region of the 2D peak (*1*), for single-layer graphene (*2*) and graphite (*3*).

3. Results and their discussion

3.1. Micropit formation under multiple irradiation

We have found that multiple irradiation with $E << E_a$ (E_a = 0.25 J cm^{-2} is the graphene damage threshold under its single irradiation [11]) may entail a local variation of the surface profile of a graphene sheet (micropit formation). The depth of these structures increases with the number of laser pulses. Figure 2a depicts the typical profile of micropits obtained in the air for RH ≈ 25%, an irradiation energy density $E_0 \approx$ 0.04 J cm^{-2} and the number of pulses $N = 6 \times 10^5$.

The resultant structure depths (1–2 nm) correspond to the depth of the adsorbed layer on the free surface of silicon dioxide in the air [12]. The thickness of the adsorbed water layer between the substrate and the graphene sheet would not be expected to change significantly in the transference of graphene to the silicon substrate in the air. Going to a more humid atmosphere would, in turn, give rise to a thicker water layer. For the same E and N values, the irradiation of a sample saturated with water in the atmosphere with RH ≈ 90% did increase the microgroove depths to 2–3 nm, i.e. twofold (see Fig. 2b).

Our attention is engaged by three more characteristic features of the resultant structures (Fig. 2). First, going to thicker adsorbed layers is accompanied by the formation of pits with a flatter bottom. Second, the lateral size of the structures is several times larger than the diameter of the irradiation spot. Third, the pits are volcano-shaped, they have 'ledges', whose heights exceed the roughness of the initial graphene surface.

3.2. Ablation-free damage (rupture) of graphene sheets

We found that at energy densities $E \gtrsim 0.048$ J cm^{-2}, which are higher than E_0, exposures to a series of laser pulses results not

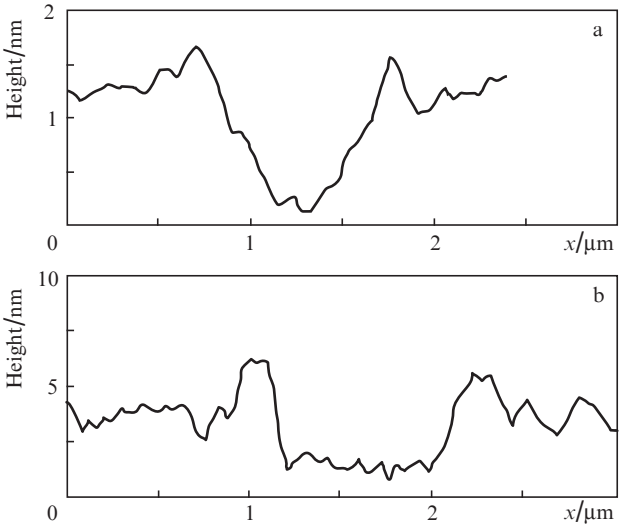

Figure 2. Cross-sectional profiles of the micropits on the graphene surface after exposing the initial sample in the air (a) and the same sample after seven-day aging in a humid atmosphere (RH = 90%) (b) to 6×10^6 pulses of focused laser radiation with an energy density of 0.04 J cm^{-2} (b).

to a profile deformation but to the damage (rupture) of graphene.

An interesting feature was observed when certain regions of graphene were irradiated by two series of laser pulses. In the first series, the energy density was $E_1 = E_0$ and in the second one it was slightly increased to some value $E_2 > E_0$, and the respective numbers of laser pulses N_1 and N_2 in each series were equal to about 6×10^5 and 6×10^4. Figure 3 shows the profiles of the graphene surface in the domain of laser irradiation in three cases: the micropit profile after the first series of pulses for $E_1 = E_0$ (Fig. 3a) and the micropit profiles after the second series of pulses for E_2 = 0.048 J cm^{-2} (Fig. 3b) and 0.058 J cm^{-2} (Fig. 3c).

With reference to Fig. 3b, when the energy density E_2 is slightly higher than E_0 there occurs only an insignificant deepening of the micropit and at the same time its broadening and a flattening of its bottom. We note: if the energy density were equal to 0.048 J cm^{-2} ($E_1 > E_0$) even in the first series, the graphene film would be damaged. Therefore, preliminary processing of graphene by low-intensity laser pulses improves its resistance to radiation damage. True, this improvement turned out to be insignificant, because the film damage was observed even for E_2 = 0.058 J cm^{-2} (Fig. 3c). Figure 4 shows the picture of radiation-induced damage, which is typical for explosive rupture of thin films.

3.3. Simulation of graphene microprofiling and rupture

The effects discussed in our work are explained in the framework of the following physical model. Lying between the graphene film and the substrate, which absorb laser radiation, the thin transparent layer of water adsorbate gets hot and boils up. The excess vapour pressure is responsible for two effects. First, it acts on the graphene film and, despite of its unique elastic properties, is capable of tearing (i.e. breaking) it, beginning with some threshold water temperature. This is observed in experiments for $E \geqslant 0.048$ J cm^{-2}. Multiple laser irradiation must result in accumulation of defects and, consequently, in lower damage thresholds. The number of laser

pulses required for damaging the film, in its turn, becomes smaller with increasing E. Second, the vapour pressure is highest on the axis of the laser beam, where the temperature of radiation-heated water is also maximal. When the vapour pressure becomes high enough, the water will be forced out to the periphery of the irradiation region. Gradually, from pulse to pulse, the water layer in the irradiation region will accordingly become thinner, with the result that the graphene film will subside under atmospheric pressure to form micropits. Their depths will increase until all water (or its major part) is removed from the region of laser irradiation. The radial expulsion of the liquid results in its excess at the boundary of the boiling region, which explains the volcano-like shape of the micropits.

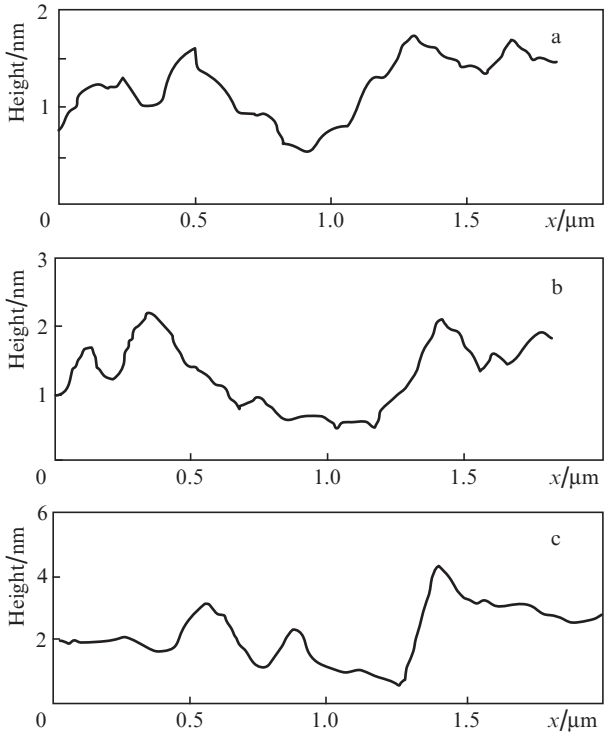

Figure 3. Cross-sectional profiles of the craters resulting after the first series of pulses with $N_1 = 6\times10^5$ for $E_1 = 0.04$ J cm^{-2} (a) as well as after additional irradiation with $N_2 = 6\times10^4$ for $E_2 = 0.048$ (b) and 0.058 J cm^{-2} (c).

To estimate the adsorbate temperature in the course of laser irradiation, we solved numerically the heat conduction equation. In doing this we took into account that the laser radiation was absorbed both in the graphene film and in silicon.

On the face of it, a significant silicon temperature growth seems to be the determining factor: $\Delta T_{Si} \approx \alpha_{Si} E/c_{Si} \approx 250^\circ$C ($\alpha_{Si} = 10^4$ cm^{-1} and $c_{Si} = 1.6$ J cm^{-3} ($^\circ$C)$^{-1}$ are the absorption coefficient and the heat capacity per unit volume, respectively, and $E = 0.04$ J cm^{-2}). However, the amorphous SiO_2 layer of thickness $H = 300$ nm, which has a low thermal diffusivity, provides a good thermal insulation of the surface layers (graphene, water adsorbate) and prevents them from being heated by silicon during the course of a laser pulse, because the condition $\exp[-H^2/(a\tau)] \ll 1$ is fulfilled ($a_{SiO_2} = 6.8\times10^{-7}$ m^{-2} s^{-1} is the thermal diffusivity of the SiO_2 layer and $\tau = 10$ ns is the duration of the laser pulse). In addition to that, crystalline silicon cools down rapidly owing to its rather high thermal diffusivity and delivers heat both to the depth of the sample and in the radial direction. If it is assumed that silicon is instantly heated by laser radiation and the radial temperature distribution $\Delta T(r)$ is Gaussian in shape, $\Delta T \propto \exp(-2r^2/w^2)$ (w is the waist radius of the laser beam), in a time τ the central ($r = 0$) temperature ΔT will decrease by a factor $(w^2/2 + a_{Si}\tau)/(w^2/2) \approx 8$ ($a_{Si} = 8.8\times10^{-5}$ m^2 s^{-1} is the thermal diffusivity of silicon) even if only the radial direction of heat transfer is taken into account (see, for instance, Ref. [13]). Consequently, after exposure to the pulse the role of rapidly cooling silicon in the heating of the adsorbed layer will be all the more insignificant.

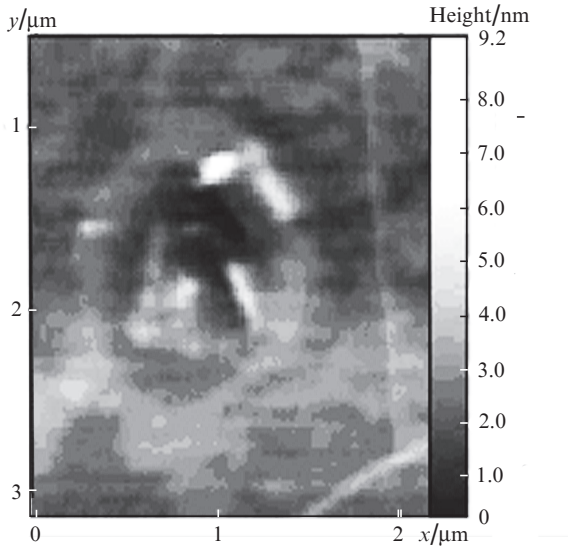

Figure 4. Crater on the surface of graphene after the exposure of its specified region by two series of laser pulses with $N_1 = 6\times10^5$ for $E_1 = 0.04$ J cm^{-2} (the first series) and with $N_2 = 6\times10^4$ for $E_2 = 0.058$ J cm^{-2} (the second series).

In view of the aforesaid, the effect of silicon was neglected in the simulations and the thermal model consisted of four-layer graphene lying on a semi-infinite SiO_2 layer covered with the adsorbate of nanometre thickness (Fig. 5), with a thermal resistance R between graphene and SiO_2 determined by the adsorbate layer.

The energy density at the centre of the laser radiation spot was assumed to be equal to 0.04 J cm^{-2}. Along the direction of

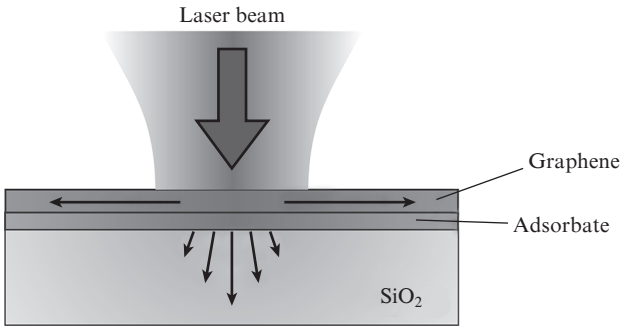

Figure 5. Model of heating and heat transfer in the graphene–substrate system.

the optical axis of laser radiation the temperature of the graphene film was assumed to be constant at each point in time. The main heat transfer directions were as follows: the radial one inside the film and vertical in going from the graphene film to the SiO_2 volume. Since the thermophysical properties of the layer of the water adsorbate at the graphene–SiO_2 interface have not been reported in the literature to date, the temperature of the thin water layer (1–2 nm in thickness) was estimated as the average of the temperatures of graphene and its adjacent surface of SiO_2.

It is well known that single-layer graphene in the absence of a substrate and adsorbate possesses a record lateral thermal conductivity of up to 5300 W m^{-1} K^{-1} [14]. However, with an increase in the number of layers the thermal conductivity becomes lower, and in the presence of a substrate it decreases further owing to the interaction of phonons with the substrate. According to Ref. [15], its experimentally measured value for a four-layer graphene on a SiO_2 substrate amounts to about 400 W m^{-1} K^{-1}. Measurements of the thermal resistance between graphene and SiO_2 yield a figure $R = 6\times10^{-9}$–1.2×10^{-7} W m^{-2} K^{-1} [16–18]. For our simulations we adopted a value of 4×10^{-8} W m^{-2} K^{-1}, which is close to the average one [16].

The fraction of radiation absorbed in graphene several (at least up to five) layers thick may be accurately calculated by the formula $\alpha = M\alpha_1$, where $\alpha_1 = 0.023$ is the fraction of radiation intensity absorbed by one layer and M is the number of graphene layers [19]. In our case, $M = 4$ and $\alpha \approx 0.1$. In these calculations, account was taken of graphene heating due to the radiation incident from the outside and the radiation reflected from the SiO_2–Si interface. The pulse shape and the spatial distribution of the laser radiation intensity were assumed to be Gaussian. Proceeding from these assumptions, the heat inflow $J(r,t)$ to the graphene film was calculated by the formula $J(r,t) = \alpha[1+ (1 - R_0)(1 - \alpha)R_{Si}]\, I_0 \exp(-t^2/\tau_e^2 - 2r^2/w^2)$, where $R_0 = 0.05$ is the reflection coefficient of SiO_2 covered with four-layer graphene [20]; $R_{Si} = 0.16$ is the reflection coefficient of the SiO_2–Si interface; I_0 is the peak intensity of the laser pulse; and $\tau_e = 5$ ns is half of pulse duration at a level 1/e.

Figure 6 shows the calculated time dependences of graphene [curve (*1*)] and water layer [curve (*2*)] temperatures at the centre of the laser spot. Shown for comparison is the time dependence of the graphene temperature calculated in the absence of the thermal flux from graphene to the substrate, i.e. for a thermal resistance $R \to \infty$ [curve (*3*)]. The variation of the laser pulse intensity in time is represented by curve (*4*). The highest temperature of the water layer amounted to about 100°C (373 K). This heating may give rise to one or several vapour cavities (bubbles) under the graphene film.

The thermal resistance of the graphene–substrate contact will sharply increase at the place of bubble emergence, which, in turn, will result in a significant increase in graphene temperature, an additional water heating and a rapid growth of the amount of vapour. To state it in different terms, when the threshold value of the energy density of laser radiation is exceeded, there emerges a positive feedback between the laser heating of graphene and the bubble formation and growth.

We also outline some additional experimental facts which, in our opinion, permit defining more precisely the mechanism of the interaction between the water adsorbate and laser radiation and explaining the cause of the slight improvement in radiation damage resistance of graphene.

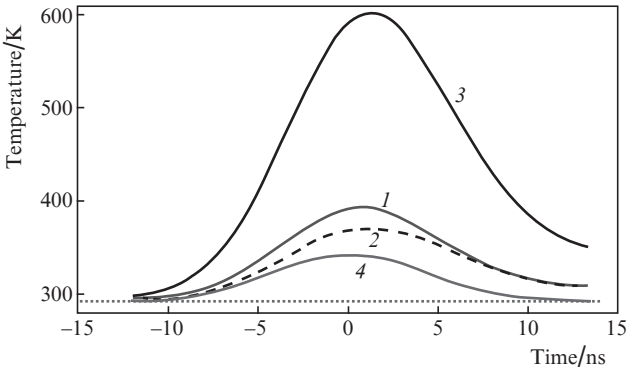

Figure 6. Heating dynamics at the centre of the irradiation spot for graphene with the inclusion of thermal contact with the SiO_2 layer (*1*), for the adsorbate layer (*2*) and for graphene in the absence of thermal contact with the SiO_2 layer (*3*). Curve (*4*) stands for the temporal dependence of laser pulse intensity (the scale for the pulse intensity is not shown in the drawing).

In small micropits, the adsorbate is forced out primarily from the central region, where the laser irradiation is most intense, which is attested by the triangular profile of such micropits (see Figs 2a and 3a). By way of comparison, in deeper micropits (which are produced at the points where the adsorbate layer is thicker) the adsorbate is forced out from the entire irradiation zone, with the result that the micropit walls become more vertical and the bottom flattens (see Fig. 2b). It is likely that the thinning of adsorbed water layer, i.e. the reduction of the number of water vapour molecules per unit area of the adsorbate layer, results in a pressure lowering in the vapour cavity produced under irradiation by a series of laser pulses. As a consequence, the process of water expulsion to the periphery of laser irradiation zone becomes less intense. That is why it is not unlikely that there persists at least a monolayer of water at the bottom of the micropit after irradiation for $E = 0.04$ J cm^{-2}. Furthermore, the reverse migration of water to under the bottom of the resultant micropit must take place upon cessation of the series of laser pulses. This phenomenon is indirectly borne out by the 'healing' of some small craters within one day after irradiation. In the interaction with higher-intensity laser radiation ($E = 0.058$ J cm^{-2}), the boiling of this remaining layer of water adsorbate results in graphene damage.

In additional experiments, the laser spot of diameter d_0 for $E = E_0$ was scanned over the surface. They showed that there formed a very small square groove with poorly discernible boundaries and a nonflat bottom (Fig. 7). The graphene surface looks like a sponge, which may be interpreted as the emergence of water islets (ice nanoparticles) at the graphene--substrate interface after laser irradiation (as is well known, water in contact with graphene is in the quasi-solid phase (ice) with tetragonal structure [21] or in the phase of 'square' ice [22]).

In the formation of separate water/ice islets at the graphene–substrate interface, their forcing out from the region of laser irradiation will be hindered by the formation of a strong Van-der-Waals bond between graphene and SiO_2 about the islets. We believe that the radiation damage resistance of graphene to pulsed laser radiation may be further improved by performing several laser irradiation series in a dry atmosphere and also by using combinations of laser and probing exposures.

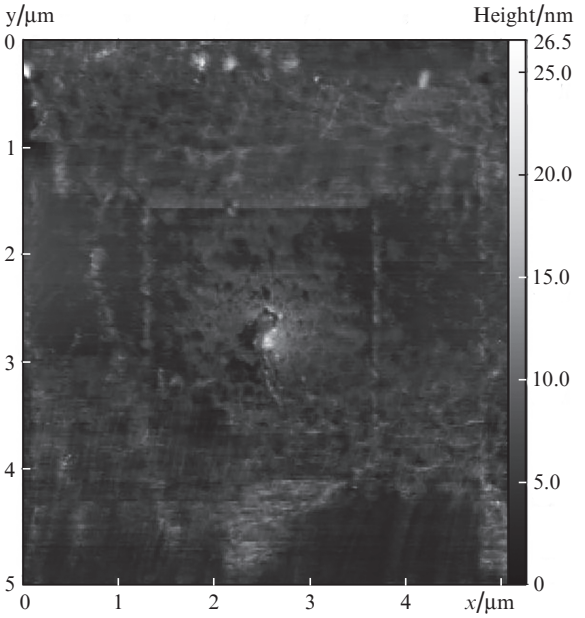

Figure 7. Graphene surface after laser beam scanning over a surface area measuring 2.5×2.5 μm for $E = 0.04$ J cm^{-2}. The edges of a square cell are discernible.

4. Conclusions

An investigation was made of a new regime of graphene profiling under low-intensity multipulse laser irradiation. This regime is underlain by the heating and boiling of the adsorbed layer between the graphene layer and substrate. In addition to its purely fundamental interest, this mode of graphene processing seems to be the only one to permit nondestructively making in graphene the separate structures and their arrays that are close to the irradiation spot diameter (no more than 1 μm) in width and are approximately 1 nm deep. An obvious disadvantage of this technology is the necessity of multiple laser irradiation (the number of pulses irradiating a given surface area amounts to 10^6). However, with the use of modern pulse-periodic solid-state lasers that generate high-intensity short laser pulses with a repetition rate of no less than 10^6 Hz and with the employment of holographic interference lithography for producing microobject arrays this disadvantage will hopefully be obviated.

Acknowledgements. This work was supported by the Russian Science Foundation (Project No. 14-22-00243).

References

1. Malenkov G. *J. Phys. Condens. Matter*, **21**, 283101 (2009).
2. Chandler D. *Nature*, **437**, 640 (2005).
3. Verdaguer A., Sacha G.M., Bluhm H., Salmeron M. *Chem. Rev.*, **106**, 1478 (2006).
4. Chaplin M.F. In: *Adsorption and Phase Behaviour in Nanochannels and Nanotubes* (London: Springer, 2010).
5. Yavari F., Kritzinger C., Gaire C., Song L., Gulapalli H., Borca-Tasciuc T., Ajayan P.M., Koratkar N. *Small*, **6**, 2535 (2010).
6. Casiraghi C., Pisana S., Novoselov K.S., Geim A.K., Ferrari A.C. *Appl. Phys. Lett.*, **98**, 233108 (2007).
7. Berciaud S., Ryu S., Brus L.E., Heinz T.F. *Nano Lett.*, **9**, 346 (2009).
8. Frolov V.D., Pivovarov P.A., Zavedeev E.V., Khomich A.A., Grigorenko A.N., Konov V.I. *Opt. Laser Technol.*, **69**, 34 (2015).
9. Ferrari A.C., Meyer J.C., Scardaci V., Casiraghi C., Lazzeri M., Mauri F., Piscanec S., Jiang D., Novoselov K.S., Roth S., Geim A.K. *Phys. Rev. Lett.*, **97**, 187401 (2006).
10. Klar P., Casiraghi C. *Phys. Status Solidi C*, **7** (11-12), 2735 (2010).
11. Dhar S., Roy Barman A., Ni G.X., Wang X., Xu X.F., Zheng Y., et al. *AIP Adv.*, **1**, 022109 (2011).
12. Asay D.B., Barnette A.L., Kim S.H. *Effect of Water Adsorption on Silicon Oxide Nano-Asperity Adhesion, in Ambient Conditions, Contact Angle, Wettability and Adhesion* (Leiden, The Netherlands: Koninklijke Brill NV, 2009) Vol. 6, p. 65.
13. Kononenko V.V., Zavedeev E.V., Latushko M.I., Konov V.I. *Laser Phys. Lett.*, **10**, 036003 (2013).
14. Balandin A.A., Ghosh S., Bao W., Calizo I., Teweldebrhan D., Miao F., Lau C.N. *Nano Lett.*, **8** (3), 902 (2008).
15. Jang W., Chen Z., Bao W., Lau C.N., Dames C. *Nano Lett.*, **10**, 3909 (2010).
16. Freitag M., Steiner M., Martin Y., Perebeinos V., Chen Z., Tsang J.C., Avouris P. *Nano Lett.*, **9**, 1883 (2009).
17. Chen Z., Jang W., Bao W., Lau C.N., Dames C. *Appl. Phys. Lett.*, **95**, 161910 (2009).
18. Shahil K.M.F., Balandin A.A. *Solid State Commun.*, **152**, 1331 (2012).
19. Nair R.R., Blake P., Grigorenko A.N., Novoselov K.S., Booth T.J., Stauber T., Peres N.M.R., Geim A.K. *Science*, **320**, 1308 (2008).
20. Skulason H.S., Gaskell P.E., Szkopek T. *Nanotechnology*, **21**, 295709 (2010).
21. Yuk J.M. et al. *Science*, **336**, 61 (2012).
22. Algara-Siller G., Lehtinen O., Wang F.C., Nair R.R., Kaiser U., Wu H.A., Geim A.K., Grigorieva I.V. *Nature (Research Letter)*, **519**, 443 (2015).